High resolution and deep tissue imaging using a near infrared acoustic resolution photoacoustic microscopy

Mohesh Moothanchery, Arunima Sharma, Vijitha Periyasamy, Manojit Pramanik*

School of Chemical and Biomedical Engineering, Nanyang Technological University, Singapore

ABSTRACT

It is always a great challenge for pure optical techniques to maintain good resolution and imaging depth at the same time. Photoacoustic imaging is an emerging technique which can overcome the limitation by pulsed light illumination and acoustic detection. Here, we report a Near Infrared Acoustic-Resolution Photoacoustic Microscopy (NIR-AR-PAM) systm with 30 MHz transducer and 1064 nm illumination which can achieve a lateral resolution of around 88 μm and imaging depth of 9.2 mm. Compared to visible light NIR beam can penetrate deeper in biological tissue due to weaker optical attenuation. In this work, we also demonstrated the *in vivo* imaging capabilty of NIR-ARPAM by near infrared detection of SLN with black ink as exogenous photoacoustic contrast agent in a rodent model.

Keywords: Acoustic resolution photoacoustic microscopy, PAM, AR-PAM, Photoacoustic imaging, Sentinel lymph node

1. Introduction

High-resolution optical imaging modalities, such as optical coherence tomography, confocal microscopy, and multiphoton microscopy, have numerous benefits. However, the spatial resolution decreases significantly as the imaging depth increases because of the diffuse nature of light transport in soft tissues [1-3]. The integration of optical excitation and ultrasound detection provides a solution to overcome the challenge of high-resolution optical imaging in deep tissues [4-8]. This approach can provide deeper imaging than other optical modalities and has been successfully applied to *in vivo* structural, functional, molecular, and cell imaging [9-17]. In PAM, a short laser pulse irradiates the tissue/sample. The absorption of light by chromophores results in a temperature increase, which in turn results in the production of pressure waves in the form of acoustics waves commonly known as photoacoustic waves. The generated photoacoustic waves can be detected by a wideband ultrasonic transducer outside the tissue boundary. Depending on the lateral resolution and imaging depth achieved, PAM can be classified as acoustic resolution photoacoustic microscopy (AR-PAM) and optical resolution photoacoustic microscopy (OR-PAM). In AR-PAM deep tissue imaging can be achieved with weak optical and tight acoustic focusing, a lateral resolution of 45 μm and an imaging depth up to 3 mm have been demonstrated [18]. OR-PAM can resolve single capillaries or even a single cell using tight optical focusing [19, 20]. In OR-PAM, the penetration depth is limited due to light focusing, and it can image up to ~1.2 mm inside the biological tissue [21, 22]. Therefore, AR-PAM can image deeper, but with a lower resolution, and OR-PAM can image with a very high resolution, but with limited imaging depth. The imaging speed of the AR and OR-PAM system mainly depends upon the pulse repetition rate of the laser source [23-25].

Not many efforts have been put to optimize the imaging depth and resolution of the AR-PAM system. Utilizing a high energy laser and a 5 MHz transducer, a lateral resolution of 590 μm and depth of 10.3 mm was demonstrated. Similarly using a 40 MHz transducer lateral resolution of 85 μm and depth of 3 mm was demonstrated

* E-mail: manojit@ntu.edu.sg

Photons Plus Ultrasound: Imaging and Sensing 2018, edited by Alexander A. Oraevsky, Lihong V. Wang, Proc. of SPIE Vol. 10494, 104945R · © 2018 SPIE · CCC code: 0277-786X/18/$18 · doi: 10.1117/12.2287838

[26]. Here we use a combination of 30 MHz focused transducer and using 1064 nm laser high lateral resolution and deep imaging was demonstrated.

2. Experimental set up

The schematic of the AR-PAM system is shown in Fig. 1 and explained in detail [27, 28]. The 1064 nm laser beam was attenuated by a neutral density filter, NDF and coupled to a multimode fiber, MMF (MHP910L02, Thorlabs). The output beam from the MMF was collimated by an Achromatic lens, L1 using a combination of objective (M-10X, Newport) and XY translator (CXY1, Thorlabs). The beam out from the fiber will pass through a collimating lens (LA1951, Thorlabs) and then the collimated beam passes through a conical lens having apex angle, 130º (Altechna, 1-APX-2-B254) to provide a ring-shaped beam. The conical lens is placed on a translating mount (CT1, Thorlabs). The ring shaped beam will be allowed to focus weakly onto the subject with the focal region coaxially overlapping the ultrasonic focus inside the tissue using a home made acrylic condenser lens having a 30 MHz ultrasonic transducer in the middle. In an optically clear medium, the optical focus will be around 2 mm in diameter, which is wider than the ultrasonic focus. The laser repetition rate will be 5 KHz and the laser energy at focus can be varied up to 1.5 mJ per pulse. The optical illumination on the object surface is donut shaped with a dark center so that no strong photoacoustic signals are produced from the surface on the object within the ultrasonic field of view. An acoustic lens of NA 0.25 was attached to the bottom of the transducer which provides an acoustic focal diameter of 80 μm

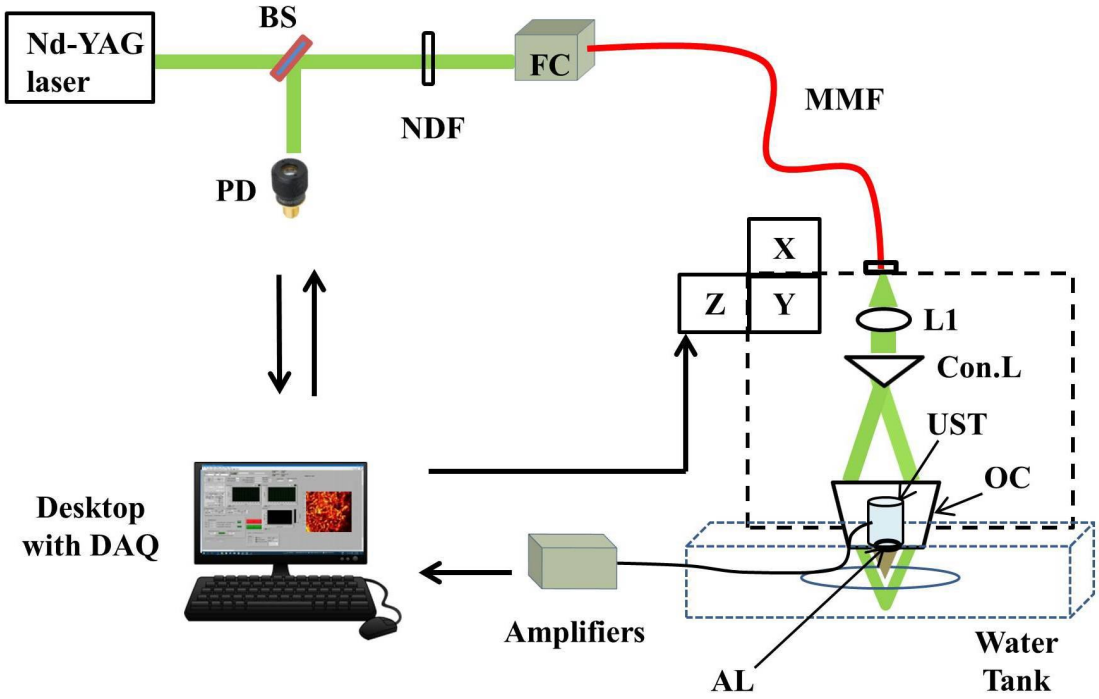

Figure 1. Schematic of the acoustic resolution photoacoustic microscopy imaging system. BS - Beam Sampler, NDF - Neutral density filter, PD – Photodiode, FC – Fiber coupler, MMF - Multimode fiber , L1 - Plano convex lens, Con.L- Conical lens , UST – Ultrasound transducer, OC - Optical condenser, DAQ - Data acquisition card

The AR-PAM scan head was attached to a 3-axis motorized stage. The bottom of the AR-PAM scanner head was submerged in a water-filled tank during photoacoustic imaging. An imaging window was opened in the bottom of the tank and sealed with a polyethylene membrane for optical and acoustic transmission. The PA signal acquired by the UST was amplified by two amplifiers having 24 dB gain each, and was recorded using a data acquisition card, DAQ in a desktop computer. The scanning and data acquisition was controlled using Labview software. Two-dimensional continuous raster scanning of the imaging head was used during image acquisition. The synchronization

of the data acquisition and the stage motion was controlled through the signal from a photodiode, PD. A beam sampler, BS was placed in front of the laser beam diverted a small portion of the beam (5%) to the PD. The PD signal was also used for compensating pulse to pulse variations during data acquisition.

3. Results and discussion

3.1 Lateral resolution and imaging depth

The lateral resolution AR-PAM system was validated using an Air Force resolution test target. Fig. 2 (a) is an 18 mm × 18 mm area MAP AR-PAM image done on a USAF 1951 test target (R1DS1P, Thorlabs). The scan step size was 2 μm and 4 μm in both X and Y direction. As from Fig. 2(a) we can see AR-PAM system is capable of clearly resolving line pairs (group 2, element 4) having 88.39 μm resolution.

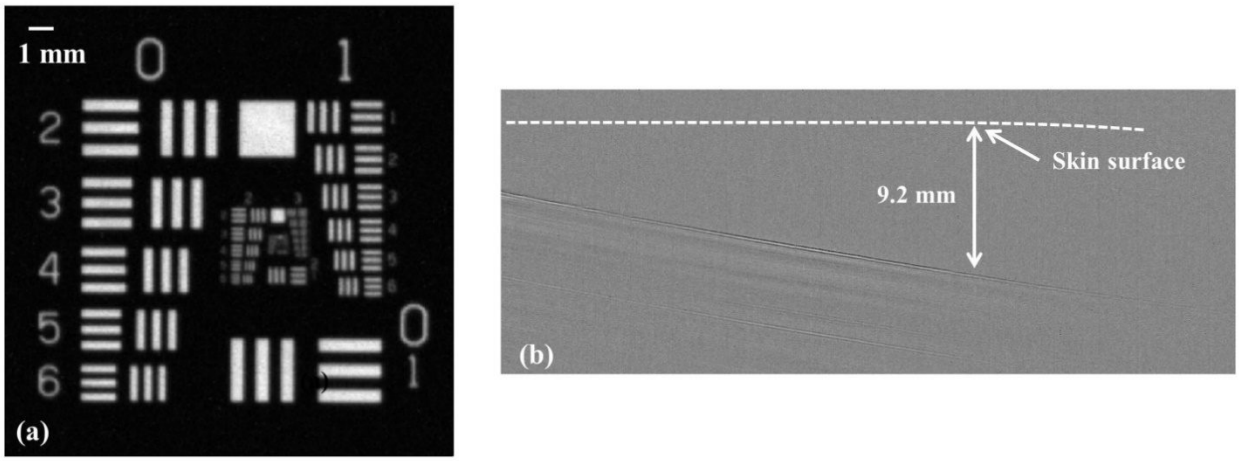

Figure.2 Lateral resolution and imaging depth measurements, (a) AR-PAM image of a USAF 1951 resolution test target, (b) single B-scan image of a black tape inserted obliquely in a chicken tissue

Theoretically, the lateral resolution for the AR-PAM will be 80μm determined using the equation $0.71 \times \lambda/\mathrm{NA}$ where λ is acoustic wavelength and NA the numerical aperture of the acoustic lens. The experimentally measured lateral resolution is slightly worse than the diffraction-limit estimate.

To determine the maximum tissue penetration a black tape was obliquely inserted on chicken tissue. From Fig. 2(b), we can clearly image the black tape down to 9.2 mm beneath the tissue surface. The laser pulse energy at the optical focus for the ARPAM systems was well below the American National Standards Institute safety limit (30 $\mathrm{mJ/cm^2}$ in the NIR spectral region).

3.2 Photoacoustic imaging of sentinel lymph node

In order to demonstrate the *in vivo* imaging capability of the system sentinel lymph node imaging was conducted. A body weight 200 ± 20 g, aged 8-10 weeks procured from InVivos Pte. Ltd. Singapore, were used in the imaging experiments. Animal experiments were performed according to the approved guidelines and regulations by the institutional Animal Care and Use committee of Nanyang Technological University, Singapore (Animal Protocol Number ARF-SBS/NIE-A0263). The animals were anesthetized using a cocktail of Ketamine (85 mg/kg) and Xylazine (15 mg/kg) injected intraperitoneally (dosage of 0.2 ml/100 gm). Figure 3(a) shows the photograph of the shaved regions of a rat for SLN imaging. Figure 3(b) shows the photograph of the shaved regions after contrast agent injection. Figure 3(c) shows the photograph of the excised sentinel lymph node after skin removal once imaging was finished.

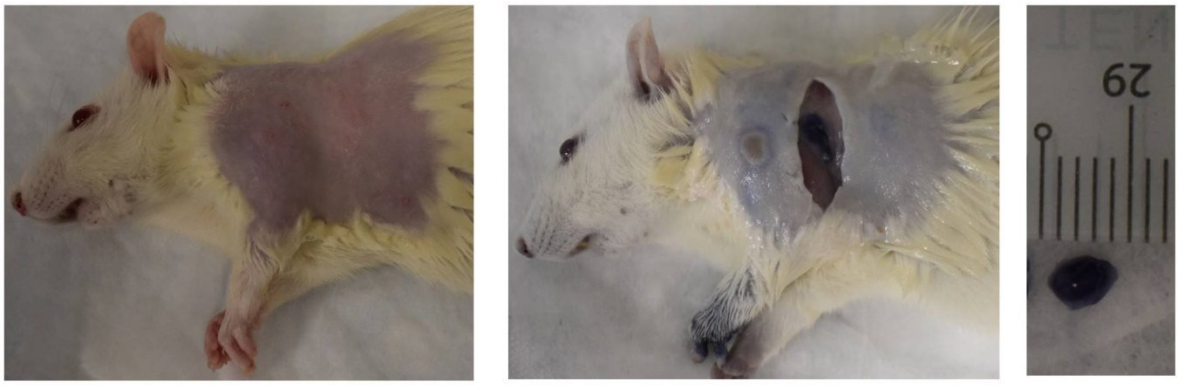

Figure 3. (a) Photograph of the shaved region of the rat for SLN imaging, (b) photograph of SLN after skin removal; (c) photograph of excised SLN.

Figure 4 (a) shows the photoacoustic maximum amplitude projection images on the shaved region before contrast agent injection. The scan area was 30 mm by 25 mm with a step size of 3 μm in the X axis and 6 μm in the Y axis. Figure 4 (b) shows similar region scanned after contrast agent injection. From Fig. 4(b) we could clearly see the SLN from the MAP images. In order to demonstrate the imaging depth 1 cm of chicken tissue was placed above the shaved region and similar scan was conducted. Figure 4(c) shows the photoacoustic maximum amplitude projection images on the shaved region with 5 mm of chicken breast tissue above the shaved region. Even with the chicken breast tissue we could clearly see the SLN from the MAP images

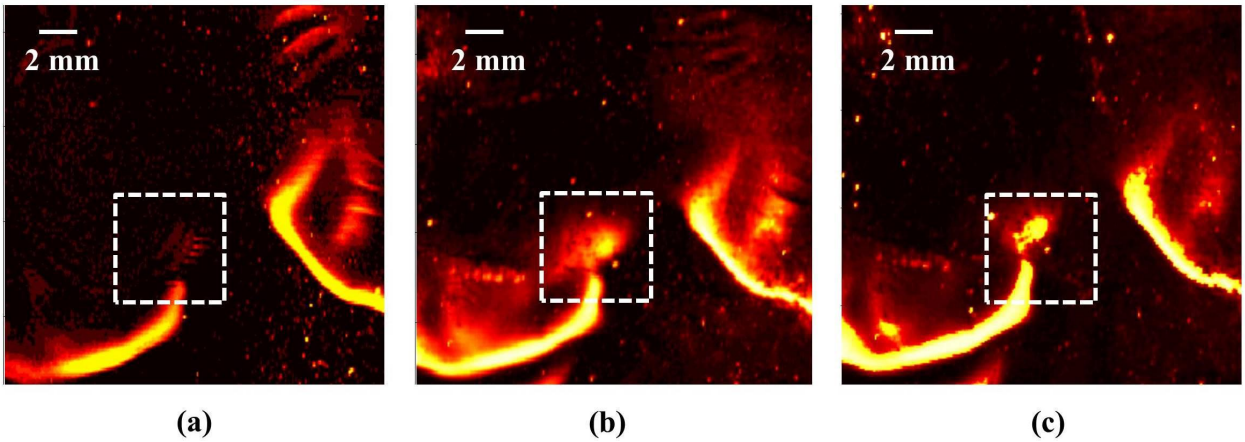

Figure 4. Photoacoutic maximum amplitude projection images (a) before black ink injection (b) after black ink injection (c) image with 5 mm CBT above the skin surface

From the MAP images in Fig.4 we could clearly visualize the SLN with contrast agent.

Conclusions

In this work, we have demonstrated an NIR AR-PAM system with high resolution and imaging depth. Lateral resolution of around 88 μm and imaging depth of 9.2 mm was successfully demonstrated using the system. The developed system was used for SLN imaging in small animals (rat). To provide imaging contrast, Black ink was used as they have high optical absorption in the visible as well as NIR wavelength region. The developed system can be used for various preclinical imaging applications where a high resolution and deep imaging is necessary.

Acknowledgements

The authors would also like to acknowledge the financial support from Tier 2 grant funded by the Singapore Ministry of Education Tier-2 Academic Research Funds (ARC2/15: M4020238).

REFERENCES

[1] W. L. V. Hu S, "Photoacoustic imaging and characterization of the microvasculature," Journal of Biomedical Optics, 15, (2010).
[2] V. Ntziachristos, "Going deeper than microscopy: the optical imaging frontier in biology," Nature Methods, 7(8), 603-14 (2010).
[3] C. L. Chen, and R. K. Wang, "Optical coherence tomography based angiography," Biomedical Optics Express, 8(2), 1056-1082 (2017).
[4] Y. Liang, L. Jin, B.-O. Guan *et al.*, "2 MHz multi-wavelength pulsed laser for functional photoacoustic microscopy," Optics Letters, 42(7), 1452-1455 (2017).
[5] M. Moothanchery, R. Z. Seeni, C. Xu *et al.*, "In vivo studies of transdermal nanoparticle delivery with microneedles using photoacoustic microscopy," Biomedical Optics Express, 8(12), 5483-5492 (2017).
[6] P. K. Upputuri, V. Periyasamy, S. K. Kalva *et al.*, "A High-performance compact photoacoustic tomography system for in vivo small-animal brain imaging," Journal of Visualized Experiments(124), e55811 (2017).
[7] R. Bi, G. Balasundaram, S. Jeon *et al.*, "Photoacoustic microscopy for evaluating combretastatin A4 phosphate induced vascular disruption in orthotopic glioma," Journal of Biophotonics, (2018) (published).
[8] P. K. Upputuri, and M. Pramanik, "Recent advances toward preclinical and clinical translation of photoacoustic tomography: a review," Journal of Biomedical Optics, 22(4), 041006 (2017).
[9] L. V. Wang, and J. Yao, "A practical guide to photoacoustic tomography in the life sciences," Nat Methods, 13(8), 627-38 (2016).
[10] Y. Zhou, J. Yao, and L. V. Wang, "Tutorial on photoacoustic tomography," Journal of Biomedical Optics, 21(6), 061007 (2016).
[11] J. Yao, and L. V. Wang, "Photoacoustic Brain Imaging: from Microscopic to Macroscopic Scales," Neurophotonics, 1(1), (2014).
[12] L. V. Wang, and S. Hu, "Photoacoustic Tomography: In Vivo Imaging from Organelles to Organs," Science, 335(6075), 1458-1462 (2012).
[13] P. Beard, "Biomedical photoacoustic imaging," Interface Focus, 1(4), 602-31 (2011).
[14] D. Pan, M. Pramanik, A. Senpan *et al.*, "Molecular photoacoustic imaging of angiogenesis with integrin-targeted gold nanobeacons," FASEB J, 25(3), 875-82 (2011).
[15] D. Pan, M. Pramanik, A. Senpan *et al.*, "Near infrared photoacoustic detection of sentinel lymph nodes with gold nanobeacons," Biomaterials, 31(14), 4088-93 (2010).
[16] L. V. Wang, "Multiscale photoacoustic microscopy and computed tomography," Nature Photonics, 3(9), 503-509 (2009).
[17] E. Z. Zhang, J. G. Laufer, R. B. Pedley *et al.*, "In vivo high-resolution 3D photoacoustic imaging of superficial vascular anatomy," Phys Med Biol, 54(4), 1035-46 (2009).
[18] H. F. Zhang, K. Maslov, G. Stoica *et al.*, "Functional photoacoustic microscopy for high-resolution and noninvasive in vivo imaging," Nature Biotechnology, 24(7), 848-51 (2006).
[19] W. Song, W. Zheng, R. Liu *et al.*, "Reflection-mode in vivo photoacoustic microscopy with subwavelength lateral resolution," Biomedical Optics Express, 5(12), 4235-41 (2014).
[20] C. Zhang, K. Maslov, S. Hu *et al.*, "Reflection-mode submicron-resolution in vivo photoacoustic microscopy," Journal of Biomedical Optics, 17(2), 020501 (2012).
[21] S. Hu, K. Maslov, and L. V. Wang, "Second-generation optical-resolution photoacoustic microscopy with improved sensitivity and speed," Optics Letters, 36(7), 1134-36 (2011).

[22] M. Moothanchery, R. Bi, J. Y. Kim *et al.*, "Optical Resolution Photoacoustic Microscopy Based on Multimode Fibers," Biomedical Optics Express, (2018) (accepted).
[23] T. J. Allen, M. O. Berendt, J. Spurrell *et al.*, "Novel fibre lasers as excitation sources for photoacoustic tomography and microscopy." 9708, 97080W.
[24] J. Yao, L. Wang, J. M. Yang *et al.*, "High-speed label-free functional photoacoustic microscopy of mouse brain in action," Nature Methods, 12(5), 407-10 (2015).
[25] J. Y. Kim, C. Lee, K. Park *et al.*, "Fast optical-resolution photoacoustic microscopy using a 2-axis water-proofing MEMS scanner," Scientific Reports, 5, 07932 (2015).
[26] M. Jeon, J. Kim, and C. Kim, "Multiplane spectroscopic whole-body photoacoustic imaging of small animals in vivo," Med Biol Eng Comput, 54(2-3), 283-94 (2016).
[27] M. Moothanchery, A. Sharma, and M. Pramanik, "Switchable Acoustic and Optical Resolution Photoacoustic Microscopy for in vivo small-animal blood vasculature imaging," Journal of Visualized Experiments(124), e55810 (2017).
[28] M. Moothanchery, and M. Pramanik, "Performance Characterization of a Switchable Acoustic and Optical Resolution Photoacoustic Microscopy System," Sensors, 17(2), 357 (2017).